

Metrology using atoms in an array of double-well potentials

Danish Ali Hamza and Jan Chwedeńczuk

Faculty of Physics, University of Warsaw, ulica Pasteura 5, 02-093 Warszawa, Poland

Quantum effects, such as entanglement, Einstein-Podolsky-Rosen steering, and Bell correlations, can enhance metrological sensitivity beyond the standard quantum limit. These correlations are typically generated through interactions between atoms or molecules, or during the passage of a laser pulse through a birefringent crystal. Here, we consider an alternative method of generating scalable, many-body entangled states, and demonstrate their usability for quantum-enhanced metrology. Our setup is a one-dimensional (1D) array of double-well potentials holding independent and uncorrelated Bose-Einstein condensates. The beam-splitting transformation mixes the signal between adjacent wells and yields a strongly entangled state through a many-body equivalent of the Hong-Ou-Mandel effect. We demonstrate this entanglement can improve the sensitivity of quantum sensors. In our analysis, we account for the effects of atomic fluctuations and identify the optimal measurement that saturates the quantum Cramer-Rao bound.

I. INTRODUCTION.

“Be precise. A lack of precision is dangerous when the margin of error is small”—Donald Rumsfeld, an American businessman and politician, once said. Same in physics—precision of measurements can be crucial. A measurement is only accurate when the sensor is highly sensitive to small changes in the observed system [1]. When restricting to classical phenomena only, the sensitivity $\Delta\theta$ of a device that measures some parameter θ and consists of N detecting particles is restricted by the Standard Quantum Limit (SQL) [2, 3]

$$\Delta\theta \geq \frac{1}{\sqrt{N}}. \quad (1)$$

If N can be arbitrarily large, then so can the sensitivity. However, the number of resources is often limited. Gravitational wave detectors cannot use lasers of infinite intensity because the sensitivity would quickly degrade due to recoil or heating of the mirrors [4]. When measuring subtle variations in gravitational acceleration or magnetic field fluctuations, one should also use small and appropriately subtle atomic, photonic, molecular or solid-state sensors [5–13].

Quantum effects come into play at this moment. In principle, one can achieve a balance between a finite N and high sensitivity by utilizing one from the triad of quantum resources: entanglement [3, 14, 15], Einstein-Podolsky-Rosen steering [16], or Bell correlations [17, 18]. The ultimate bound is the Heisenberg limit (HL) [15, 19]

$$\Delta\theta \geq \frac{1}{N}. \quad (2)$$

To reach the HL, the most subtly correlated quantum states must be used. However, due to the immediate decoherence, it is rather elusive [20]. Therefore whenever an improvement to the SQL is demonstrated, i.e., $\Delta\theta < \frac{1}{\sqrt{N}}$, it is considered a major achievement. Entanglement in multi-qubit systems is often generated by spin squeezing the sample [21–28]. Another method is to use two-body collisions of atoms to create an intense source

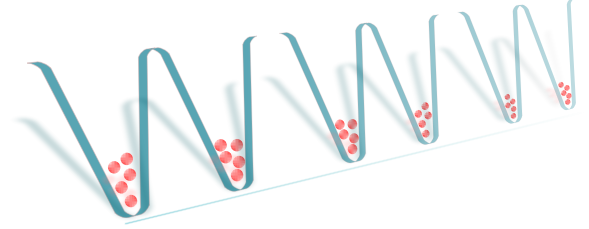


FIG. 1. This is an illustration of the interferometric setup of interest in this work. It shows a collection of M double wells, each of which is filled with an ultra-cold bosonic gas.

of entangled pairs [29–37] in analogy to the well-known optical parametric down-conversion process [38, 39].

Sensitivity can also be improved by increasing the signal dependent on θ . In gravitational-wave detection, the signal is amplified using the large, 4-kilometer-long arms of the Michelson interferometer [4]. For measurements of a local gravitational acceleration, the two atomic beam trajectories are separated as far as matter-wave coherence constraints allow [40–45]. In this vein is the recent series of experiments involving a one-dimensional array of double-well (DW) potentials that trap ultra-cold bosonic atoms, schematically shown in Fig. 1. The array is lengthy; therefore, if each DW acts as an interferometer measuring θ , the overall precision can be high. Long-range coherence has been demonstrated in this system through the observation of long-lived Bloch oscillations [46]. Recently, this system was used for the first time to precisely measure gravitational acceleration [47].

This manuscript aims to explain how the sensitivity of the multi-DW interferometer increases due to the interplay between its large size and quantum correlations. First, we introduce the model in Section II A. Next, Section II B briefly discusses the main tool that determines sensitivity: the Quantum Fisher Information (QFI). In Section II C we derive the ultimate bounds (i.e., the SQL and the HL) for this system. This part of the manuscript concludes with the discussion of mode mixing, which is equivalent to an inter-DW beam-splitter, see

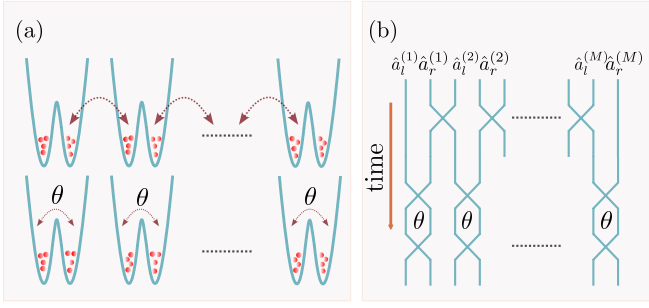


FIG. 2. (a): The illustration of the interferometric procedure. The top row shows the mixing of modes of adjacent double wells. The bottom one depicts the imprinting of parameter θ using the collection of M independent Mach-Zehnder interferometers. (b): Schematic representation showing the two steps brought together to form a time sequence.

Section II D. This mixing creates a nontrivial multimode state across the array by correlating the modes. The next section discusses the impact of this mixing on sensitivity. We demonstrate that, even when an interferometer is supplied with a product of “semiclassical” atomic states, bosonic interference at the beam splitter can enhance sensitivity (see Section III A). This is a many-body analog of the Hong-Ou-Mandel (HOM) effect [48]. Next, in Section III B, we compare this result to the case in which the interferometer is fed by a collection of entangled states obtained through the one-axis twisting (OAT) procedure. It is a well-known method for producing highly entangled and even Bell-correlated states, which are useful for quantum metrology [24, 49]. This is why we are interested in this technique. In Section III C we illustrate the impact of shot-to-shot atom number fluctuations on the sensitivity. The Appendix follows the conclusions. We moved some of the details of the analytical calculations there for the sake of clarity in the manuscript.

II. MODEL

In this section, we will discuss the basic building blocks of the multi-DW interferometer: state, sensitivity, and allowed transformations.

A. The state

The system under consideration is comprised of N bosonic particles of a single species, which are distributed across M double-well potentials, forming a 1D array, as illustrated in Fig. 1. The full Hilbert space \mathcal{H} is spanned by Fock states

$$|\vec{n}\rangle = |n_l^{(1)}, n_r^{(1)} \dots n_l^{(M)}, n_r^{(M)}\rangle, \quad (3)$$

where $n_{l/r}^{(i)}$ is the number of bosons in the left/right mode of the i -th well with the constraint

$$\sum_{i=1}^M (n_l^{(i)} + n_r^{(i)}) = N. \quad (4)$$

In this configuration, any quantum state can be represented as

$$\hat{\rho} = \sum_{\vec{n}, \vec{n}'} \varrho_{ij} |\vec{n}\rangle \langle \vec{n}'|. \quad (5)$$

Nevertheless, it is challenging to work with states of this form, as the dimension of \mathcal{H} is too large to address the problem, even when N and M are moderate. The focus henceforth will be restricted to an experimentally substantiated case. Initially, the double-wells form separate subsystems, each occupied by n bosons, so that $nM = N$. This vastly simplifies the analysis as now any quantum state can be expressed as follows

$$\hat{\rho} = \sum_m p_m \hat{\rho}_1^{(m)} \dots \hat{\rho}_M^{(m)}, \quad (6)$$

where $p_m \geq 0$ and $\sum_m p_m = 1$, while each of the “local” density operators can be expressed by means of vectors $|n_r, n - n_r\rangle$. While the focus will be on pure input states in establishing upper bounds for the sensitivity, mixed state will be considered in the context of potential experimental imperfections.

B. The tool: Quantum Fisher Information

Inspired by a recent experimental work [47] we consider M Mach-Zehnder interferometers, feeding independently each DW with the information about an unknown parameter θ . This can be expressed in terms of a unitary transformation of an input state $\hat{\rho}$, as follows:

$$\hat{\rho}(\theta) = e^{-i\theta \hat{J}_y} \hat{\rho} e^{i\theta \hat{J}_y}, \quad (7)$$

where the collective operator is

$$\hat{J}_y \equiv \sum_{i=1}^M \hat{J}_y^{(i)}. \quad (8)$$

and the individual single-DW operators are defined as follows

$$\hat{J}_y^{(i)} = \frac{1}{2i} (\hat{a}_r^{(i)\dagger} \hat{a}_l^{(i)} - \hat{a}_l^{(i)\dagger} \hat{a}_r^{(i)}). \quad (9)$$

The operators $\hat{a}_{l/r}^{(i)}$ annihilate a boson in the left/right well of the i -th DW. A transformation like in Eq. (7) can be triggered by a linear external potential acting on the system, so the scenario here could be relevant to precise gravimetry of the local gravitational acceleration g [47].

Once the output state is generated, some measurements yield the estimated parameter with an uncertainty $\pm\Delta\theta$. Its minimal value is given by the quantum Cramer-Rao lower bound (QCRB)

$$\Delta\theta \geq \frac{1}{\sqrt{\mathcal{I}_q[\hat{\rho}(\theta)]}}, \quad (10)$$

where $\mathcal{I}_q[\hat{\rho}(\theta)]$ is the quantum Fisher information (QFI) that reads [1]

$$\mathcal{I}_q[\hat{\rho}(\theta)] = 2 \sum_{i,j} \frac{1}{p_i + p_j} |\langle \psi_i | \dot{\hat{\rho}}(\theta) | \psi_j \rangle|^2. \quad (11)$$

Here, the dot denotes the derivative of the density matrix from Eq. (7) over θ and $|\psi_{i/j}\rangle$ are the eigen-vectors of the density matrix $\hat{\rho}(\theta)$ with the corresponding eigen-values $p_{i/j}$. The double sum runs through all the non-trivial part of the spectrum, i.e., whenever $p_i + p_j \neq 0$.

The analytical evaluation of the QFI, necessary to establish the QCRB from Eq. (10), is usually impossible as the analytical diagonalization of the θ -dependent density matrix is hardly ever possible. However, a major simplification comes from the following inequality [1]

$$\mathcal{I}_q[\hat{\rho}(\theta)] \leq 4\Delta^2 \hat{J}_y \equiv 4 \left(\langle \hat{J}_y^2 \rangle - \langle \hat{J}_y \rangle^2 \right) \leq 4\langle \hat{J}_y^2 \rangle, \quad (12)$$

where the averages are calculated using $\langle \cdot \rangle = \text{Tr}[\hat{\rho}(\theta) \cdot]$. This inequality is saturated if the density matrix $\hat{\rho}(\theta)$ represents a pure state. Consequently, in order to establish the upper bounds for the sensitivity, it is essential to identify the optimal pure states. In the following section, we will proceed with a detailed analysis of this concept.

C. Ultimate scalings

We begin by establishing a shot-noise limit for this system. This will allow us to track any quantum enhancements due to the entanglement of the input state of the collective Mach-Zehnder interferometer. A separable state will be one that does not exhibit quantum correlations among the DWs, i.e., such as in Eq. (6). Moreover, the two-mode n -boson density matrix of every DW, $\hat{\rho}_i$, must represent a “classical” state. The basic building block of such a $\hat{\rho}_i$ is called a coherent spin state (CSS), which reads

$$|\theta_i, \varphi_i\rangle = \frac{1}{\sqrt{n!}} \left(\hat{b}^{(i)\dagger} \right)^n |0\rangle. \quad (13)$$

It is simply a Fock state, obtained with an n -fold action of a creation operator

$$\hat{b}^{(i)\dagger} = \hat{a}_r^{(i)\dagger} \cos \theta_i + \hat{a}_l^{(i)\dagger} \sin \theta_i e^{i\varphi_i} \quad (14)$$

with $\theta_i \in [0, \pi[$ and $\varphi_i \in [0, 2\pi[$, on the two-mode vacuum $|0\rangle$. States (13) can be used to construct any separable single-DW state in the form

$$\hat{\rho}_i = \int_0^\pi d\theta_i \int_0^{2\pi} d\varphi_i \mathcal{P}(\theta_i, \varphi_i) |\theta_i, \varphi_i\rangle \langle \theta_i, \varphi_i|, \quad (15)$$

where \mathcal{P} is any probability distribution of variables θ_i and φ_i . Subsequently, a separable state of M double-wells is constructed as a product

$$\hat{\rho}_{sep} = \bigotimes_{i=1}^M \hat{\rho}_i. \quad (16)$$

Finally, one can consider a statistical mixture of such product states, as in Eq. (6), where m labels the different probability distributions $\mathcal{P}^{(m)}(\theta_i, \varphi_i)$. In this way, the most general separable state is constructed.

This state sets a reference value of the sensitivity as it gives

$$\Delta\theta \geq \frac{1}{\sqrt{M}} \frac{1}{\sqrt{n}} = \frac{1}{\sqrt{N}}, \quad (17)$$

i.e., a shot-noise scaling with the total number of resources, N , or a “double” shot-noise scaling with the number of DWs, M , and the number of atoms per DW, n .

Values of $\Delta\theta$ that are smaller than the SQL of Eq. (17) imply the presence of some form of entanglement in the system. For example, $\hat{\rho}$ might still be expressed as in Eq. (6) but at least one of the local states could be non-separable, which means it could not be expressed as in Eq. (15). The limiting value of the sensitivity for such a case is obtained when the interferometer is fed with a product of M NOON states

$$|\psi^{(i)}\rangle = \frac{1}{\sqrt{2}} (|n, 0\rangle_y^{(i)} + |0, n\rangle_y^{(i)}), \quad (18)$$

giving the Heisenberg scaling with n , namely

$$\Delta\theta = \frac{1}{\sqrt{M}} \frac{1}{n}. \quad (19)$$

Here, the two components of the superposition (18) are the eigenstates of $\hat{J}_y^{(i)}$ with the maximal/minimal eigenvalue, namely

$$\hat{J}_y^{(i)} |n, 0\rangle_y^{(i)} = \frac{n}{2} |n, 0\rangle_y^{(i)}, \quad (20a)$$

$$\hat{J}_y^{(i)} |0, n\rangle_y^{(i)} = -\frac{n}{2} |0, n\rangle_y^{(i)}. \quad (20b)$$

The “intra-entanglement” depicts situations when the state cannot be represented in the form of Eq. (6). The DWs become entangled and a global NOON state

$$|\psi\rangle = \frac{1}{\sqrt{2}} \left(\bigotimes_{i=1}^M |n, 0\rangle_y^{(i)} + \bigotimes_{i=1}^M |0, n\rangle_y^{(i)} \right), \quad (21)$$

gives the global Heisenberg scaling with the total number of resources, i.e.,

$$\Delta\theta = \frac{1}{M} \frac{1}{n} = \frac{1}{N}. \quad (22)$$

The values of $\Delta\theta$ in the range between Eqs (17) and (22) are the “playground” for quantum-enhanced metrology

with a collection of DWs. The pair of states, Eqs (18) and (21), that saturate (19) and (22) respectively, set a reference, but should not be pursued as an achievable goal. Despite impressive progress made in trapped atom interferometry, including the multi-DW setup [46, 47], the entangled systems that can be generated at present (or in the nearby future) are a far cry from those NOON states. Therefore in the next section we propose a modification of the MZI sequence of Eq. (7) that still beats the SQL but using CSSs at the input.

D. Mode mixing

Consider an additional operation, equivalent to a beam splitter, that couples the right mode of the i -th DW with the left mode of the $(i + 1)$, as shown schematically in Fig. 2(a). It is generated by

$$\hat{S}_x^{(i)} = \frac{1}{2} \left(\hat{a}_r^{(i)\dagger} \hat{a}_l^{(i+1)} + \hat{a}_l^{(i+1)\dagger} \hat{a}_r^{(i)} \right). \quad (23)$$

The collective beam-splitter operator is thus

$$\hat{S}_x = \sum_{i=1}^{M-1} \hat{S}_x^{(i)} \quad (24)$$

(the truncation of the sum at $i = M - 1$ is a consequence of open boundary conditions). We assume that this transformation precedes the MZI interferometers and modifies the input state as follows:

$$\hat{\rho} \longrightarrow e^{-i\frac{\pi}{2}\hat{S}_x} \hat{\rho} e^{i\frac{\pi}{2}\hat{S}_x}. \quad (25)$$

Subsequently, this density matrix is fed into the collection of MZIs, see Eq. (7).

For convenience, it is preferable to switch from the Schrödinger picture [see Eq. (25)] to the Heisenberg picture and evolve the generator of the MZI transformation, Eq. (8), namely

$$\hat{S}_y \equiv e^{i\frac{\pi}{2}\hat{S}_x} \hat{J}_y e^{-i\frac{\pi}{2}\hat{S}_x} \quad (26)$$

or equivalently

$$\hat{S}_y^{(i)} \equiv e^{i\frac{\pi}{2}\hat{S}_x} \hat{J}_y^{(i)} e^{-i\frac{\pi}{2}\hat{S}_x}. \quad (27)$$

By inspecting the expression for the mixing operator \hat{S}_x , Eq. (23), we obtain the pairs of left / right annihilation operators that couple to its closest neighbours

$$\hat{a}_{(l),out}^{(i-1)} = \frac{\hat{a}_l^{(i-1)} - i\hat{a}_r^{(i)}}{\sqrt{2}}, \quad (28a)$$

$$\hat{a}_{(r),out}^{(i)} = \frac{\hat{a}_r^{(i)} - i\hat{a}_l^{(i-1)}}{\sqrt{2}}. \quad (28b)$$

Consequently, the internal operators labelled with $i \neq 1, M$ (i.e., those that couple to the neighbours at both sides) take the following form:

$$\hat{S}_y^{(i)} = \frac{1}{2} \left(\hat{J}_y^{(i)} + \hat{Y}_y^{(i)} + \hat{R}^{(i)} - \hat{L}^{(i+1)} \right). \quad (29)$$

where the three new operators are

$$\hat{L}^{(i)} = \frac{1}{2} \left(\hat{a}_l^{(i-1)\dagger} \hat{a}_l^{(i)} + \hat{a}_l^{(i-1)} \hat{a}_l^{(i)\dagger} \right) \quad (30a)$$

$$\hat{R}^{(i)} = \frac{1}{2} \left(\hat{a}_r^{(i-1)\dagger} \hat{a}_r^{(i)} + \hat{a}_r^{(i-1)} \hat{a}_r^{(i)\dagger} \right) \quad (30b)$$

$$\hat{Y}^{(i)} = \frac{1}{2i} \left(\hat{a}_l^{(i-1)\dagger} \hat{a}_r^{(i+1)} - \hat{a}_r^{(i+1)\dagger} \hat{a}_l^{(i-1)} \right). \quad (30c)$$

Finally, the extreme operators, i.e., for $i = 1$ and $i = M$ transform into

$$\hat{S}_y^{(1)} = \frac{1}{\sqrt{2}} \left(\hat{J}_y^{(1)} - \hat{L}^{(2)} \right), \quad (31a)$$

$$\hat{S}_y^{(M)} = \frac{1}{\sqrt{2}} \left(\hat{J}_y^{(M)} + \hat{R}^{(M)} \right). \quad (31b)$$

We are now prepared to compute the sensitivity for the mixing / MZI protocol with some semi-classical input states.

III. BREAKING THE SQL

Using the expressions from Eqs (12) and (27) we obtain

$$\mathcal{I}_q = 4 \sum_{i=1}^M \Delta^2 \hat{S}_y^{(i)} + 8 \sum_{i \neq j=1}^M \left(\langle \hat{S}_y^{(i)} \hat{S}_y^{(j)} \rangle - \langle \hat{S}_y^{(i)} \rangle \langle \hat{S}_y^{(j)} \rangle \right) \quad (32)$$

which is used below to establish the QCRB for pure states.

A. Coherent spin states

First, we consider the CSS, see the definition in Eq. (13), with $\theta_i = 0$ for all i . This corresponds to

$$|\psi\rangle = \bigotimes_{i=1}^M |0, n\rangle_i. \quad (33)$$

Such a state is an idealization of a setup, where M independent BECs are loaded into every second site of a multi-DW system. In contrast to a realistic scenario, it neglects the shot-to-shot atom-number fluctuations, which will be discussed in the next section. Using Eq. (32) we obtain [see Appendix A for details]

$$\mathcal{I}_q = \frac{1}{2} M(n^2 + 2n). \quad (34)$$

Though the sensitivity scales at the SQL with the number of DWs, M , it exceeds the classical bound as a function of n [compare with Eq. (17)]. The inter-DW mixing is nonlocal in terms of DWs, hence it disturbs the structure of Eqs (15) and (16). This improves the sensitivity through a many-body equivalent of the Hong-Ou-Mandel effect [48, 50], which is known in quantum optics. In our

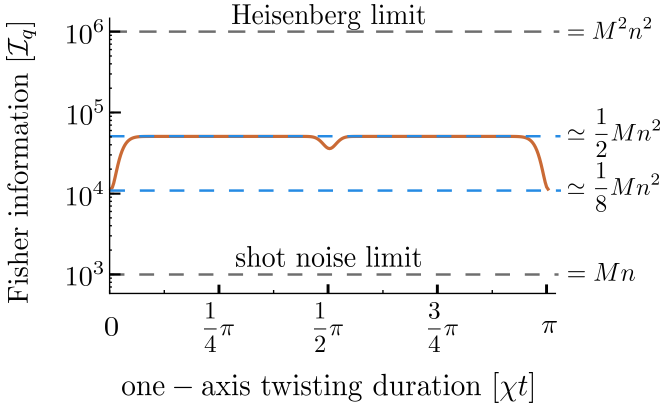


FIG. 3. The QFI \mathcal{I}_q calculated with $M = 10$ DWs, each initially loaded with $n = 100$ atoms. The gray dashed lines at the top and bottom show the HL and SQL, respectively. The two blue dashed lines in the center show the sensitivities that can be achieved using coherent states, as defined by Eq. (33) (upper) and Eq. (36) (lower line). The solid red line shows the QFI obtained using the output of the OAT procedure, Eq. (39), as a function of its duration χt .

case, the mixing distributes the bosons across the neighboring DWs. The subsequent first beam-splitter opening the MZI plays the role analogue to the beam-splitter in the two-photon HOM effect—interference of bosons yields a non-classical state [51–55].

Another way of loading M BECs into the array of DWs is by distributing each set of n bosons coherently and symmetrically among the two sites. This corresponds to a product of single-DW CSSs, as in Eq. (13) with $\theta_i = \frac{\pi}{2}$ and $\varphi_i = 0$ for all i , namely

$$\begin{aligned} |\phi^{(i)}\rangle &= \frac{1}{\sqrt{n!}} \left(\frac{\hat{a}_r^{(i)\dagger} + \hat{a}_l^{(i)\dagger}}{\sqrt{2}} \right)^n |0\rangle_i \\ &= \sum_{m_i=0}^n \sqrt{\frac{1}{2^n} \binom{n}{m_i}} |m_i, n - m_i\rangle_i, \end{aligned} \quad (35)$$

giving the composite state

$$|\phi\rangle = \bigotimes_{i=1}^M |\phi^{(i)}\rangle. \quad (36)$$

Using Eq. (32) we obtain the QCRB [again, see Appendix A for the details of the derivation]

$$\mathcal{I}_q = \frac{1}{8} M n^2 + \frac{1}{2} (1 - \sqrt{2}) n^2 + \frac{1}{4} \left(\frac{7}{2} M + 1 \right) n. \quad (37)$$

Also in this case, the sensitivity surpasses the SQL with the dominant (for large n and M) scaling $\mathcal{I}_q \sim \frac{1}{8} M n^2$.

B. One-axis twisting

These two CSSs show that even when the input of the multi-DW interferometer is a set of independent semi-

classical atomic states, the SQL can still be surpassed. For reference, we calculate the QCRB for the case when the input is composed of M independent but entangled states. To control the strength of entanglement, we consider the one-axis twisting protocol, where each state, initially as in Eq. (35), undergoes the following dynamics

$$|\psi^{(i)}(t)\rangle = \sum_{m_i=0}^n e^{-i\chi t m_i^2} \sqrt{\frac{1}{2^n} \binom{n}{m_i}} |m_i, n - m_i\rangle_i. \quad (38)$$

This type of evolution is generated by the two-body collisions quantified by the coupling constant χ . Once the locally entangled state is prepared, the input of the mixing/MZI dynamics is

$$|\psi(t)\rangle = \bigotimes_{i=1}^M |\psi^{(i)}(t)\rangle. \quad (39)$$

The QCRB calculated with this state and Eq. (32) gives a complicated formula which we reproduce in full extent in the Appendix A. Nevertheless, at most of the times t such that χt is not an integer multiple of $\pi/2$, the \mathcal{I}_q vastly simplifies as the quickly oscillating phase terms $e^{-i\chi t m_i^2}$ average to zero giving

$$\mathcal{I}_q \sim \frac{1}{2} M n^2. \quad (40)$$

Hence in our scenario this complex entangling procedure does not give any improvement when compared to the performance of M separable states, see Eq. (34). This observation could simplify future implementations of the multi-DW scheme discussed in this work.

To summarize the results of this section, in Fig. 3 we display the performance of the OAT state, as a function of χt for $n = 100$ and $M = 10$. This is compared with the SQL and the HL, see Eqs (17) and (22) respectively. The two other distinct values, $\mathcal{I}_q = \frac{1}{2} M n^2$ and $\mathcal{I}_q = \frac{1}{8} M n^2$, achievable with the CSSs are shown for reference. The take-away message is that the use of CSS, accompanied by the inter-DW mixing, can yield very high sensitivity, thanks to the many-body HOM effect.

C. Atom Number Fluctuations

Since the BEC loaded into just one site of a DW, Eq. (33), gives a very good scaling with n , see Eq. (34), we focus on this scenario and scrutinize the impact of shot-to-shot atom fluctuations. Now, each DW is loaded with a mixture

$$\hat{\rho}_i = \sum_{m_i=0}^n p(m_i) |m_i, n - m_i\rangle \langle m_i, n - m_i|, \quad (41)$$

and, for illustration, we use the Gaussian probability

$$p(m_i) = \mathcal{N} e^{-\frac{m_i^2}{2\sigma^2}}, \quad (42)$$

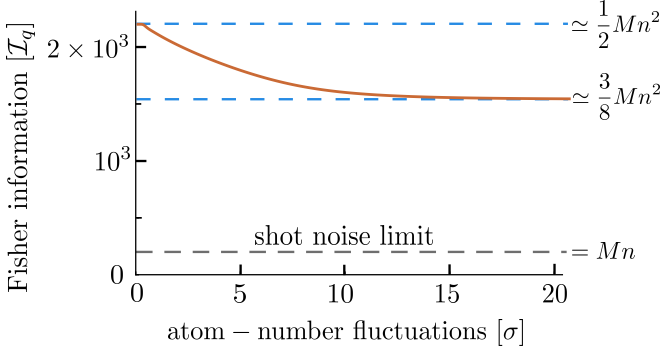


FIG. 4. Red solid line; the QFI as a function of the strength of the shot-to-shot atom fluctuations σ , as given by Eq. (42) with $n = 20$ and $M = 10$. The dashed gray line at the bottom shows the SQL. The top dashed line denotes the value of \mathcal{I}_q which is attained in the absence of fluctuations, see Eq. (34). The central dashed line is the analytical result for $\sigma \rightarrow \infty$, see Eq. (43).

where \mathcal{N} is the normalization constant that depends on the strength of the shot-to-shot fluctuations σ . Now, the BEC can be incoherently distributed among the two sites. We feed the mixing/MZI protocol with a product of $M = 10$ such states, each with $n = 20$ atoms and calculate the \mathcal{I}_q numerically, using the general expression from Eq. (11). The result is displayed in Fig. 4 together with the SQL and the two limiting cases. One is for $\sigma \rightarrow 0$, when the numerical computation recovers the formula from Eq. (34). The other is for $\sigma \rightarrow \infty$, where the analytical result shows that

$$\lim_{\sigma \rightarrow \infty} \mathcal{I}_q = \frac{n^2 + 2n}{8} (3M - 2) \simeq \frac{3}{8} M n^2. \quad (43)$$

Hence even large shot-to-shot fluctuations of the BEC distribution among the two sites do not kill the sub shot-noise scaling of the QCRB. All the intermediate steps of the calculation leading to the above result are presented in Appendix B.

D. Optimal measurement

In this final section we show that the measurement of the number of particles in each site and the subsequent estimation of θ from the probability distribution of these outcomes is optimal for any input state that has real coefficients and when working around $\theta = 0$. This applies to both the pure CSSs considered in the previous section. By “optimal”, we mean that the sensitivity for this particular estimation protocol saturates the QCRB.

Let $|\psi_{in}\rangle$ be an input state of the MZI interferometer. We consider a general state and hence do not specify if the inter-DW mixing was performed. The probability of finding the output state

$$|\psi(\theta)\rangle = e^{-i\theta \hat{J}_y} |\psi_{in}\rangle \quad (44)$$

in any of the states from Eq. (3) is

$$p(\vec{n}|\theta) = |\langle \vec{n} | \psi(\theta) \rangle|^2. \quad (45)$$

From this probability, the parameter θ can be estimated with the maximal sensitivity as in Eq. (10) but with $\mathcal{I}_q[\hat{\rho}(\theta)]$ replaced by

$$\mathcal{I}_{cl} = \sum_{\vec{n}} \frac{1}{p(\vec{n}|\theta)} \left(\frac{\partial p(\vec{n}|\theta)}{\partial \theta} \right)^2. \quad (46)$$

Taking $\theta = 0$ as a working point, around which the derivative is calculated, we obtain that, for all the states $|\psi_{in}\rangle$ with real coefficients of the expansion into the basis of $|\vec{n}\rangle$, namely $\langle \vec{n} | \psi_{in} \rangle$, the probability is

$$p(\vec{n}|0) = \langle \vec{n} | \psi_{in} \rangle^2. \quad (47)$$

For this case, the derivative of the probability is

$$\left. \frac{\partial p(\vec{n}|\theta)}{\partial \theta} \right|_{\theta=0} = i \langle \vec{n} | \psi_{in} \rangle \left(\langle \vec{n} | \hat{J}_y | \psi_{in} \rangle - \langle \psi_{in} | \hat{J}_y | \vec{n} \rangle \right). \quad (48)$$

Plugging this expression into Eq. (46) we obtain

$$\mathcal{I}_{cl} = \sum_{\vec{n}} \left(2 |\langle \vec{n} | \hat{J}_y | \psi_{in} \rangle|^2 - \langle \vec{n} | \hat{J}_y | \psi_{in} \rangle^2 - \langle \psi_{in} | \hat{J}_y | \vec{n} \rangle^2 \right) \quad (49)$$

Taking the first term separately, we note that the sum over \vec{n} can be performed giving

$$\sum_{\vec{n}} |\langle \vec{n} | \hat{J}_y | \psi_{in} \rangle|^2 = \langle \hat{J}_y^2 \rangle, \quad (50)$$

where the average is calculated in the input state $|\psi_{in}\rangle$. As for the latter two terms, we have

$$\begin{aligned} \langle \vec{n} | \hat{J}_y | \psi_{in} \rangle^2 + \langle \psi_{in} | \hat{J}_y | \vec{n} \rangle^2 &= \\ &= \left(\langle \vec{n} | \hat{J}_y | \psi_{in} \rangle + \langle \psi_{in} | \hat{J}_y | \vec{n} \rangle \right)^2 - 2 |\langle \vec{n} | \hat{J}_y | \psi_{in} \rangle|^2. \end{aligned} \quad (51)$$

Hence the CFI is equal to

$$\mathcal{I}_{cl} = 4 \langle \hat{J}_y^2 \rangle - 4 \sum_{\vec{n}} \left(\text{Re} \left[\langle \vec{n} | \hat{J}_y | \psi_{in} \rangle \right] \right)^2 \quad (52)$$

Real coefficients of the input state imply that $\text{Re} \left[\langle \vec{n} | \hat{J}_y | \psi_{in} \rangle \right] = 0$ [due to the presence of the imaginary unit in the definition of \hat{J}_y , see Eq. (9)], hence we obtain that

$$\mathcal{I}_{cl} = 4 \langle \hat{J}_y^2 \rangle, \quad (53)$$

which saturates Eq. (12). Hence, the measurement of the population imbalance is optimal as the \mathcal{I}_{cl} saturates the QCRB for $|\psi\rangle$'s that have real coefficients of the expansion in the basis of eigen-states of \hat{J}_z .

IV. CONCLUSIONS

In this manuscript, we presented an analysis of a composite interferometer operating on a collection of DWs. We calculated the ultimate scaling with respect to the number of particles and the number of DWs that can be achieved with this setup. Next, we introduced the inter-DW mixing which enables high sensitivity even when the array is loaded with a collection of semiclassical states. The many-body equivalent of the HOM effect is potent and resilient in the face of atomic fluctuations. Additionally, we demonstrated that the estimation obtained by measuring the number of atoms in each DW is optimal, meaning it saturates the QCRB.

The improvement from using CSSs and mixing is expressed in terms of an HL scaling with n . To obtain sub-SQL sensitivities in terms of M as well, long-range coherence must be established in the system. For this purpose, other than nearest-neighbor beam-splitter operations should be considered.

Of course, the discussion presented here is only the

first step in a complete analysis of the interferometric performance of this setup. A more realistic scenario is one in which the atom-number measurements are imprecise. Phase noise can cause fluctuations in the relative depth of the DWs. The number of particles in each DW and the total number of particles can also fluctuate from shot to shot. Other sources of decoherence can further reduce precision. Nevertheless, we hope that the results presented in this work will inspire further research on this novel, promising interferometric scheme.

ACKNOWLEDGEMENTS

This work was supported by the National Science Centre, Poland, within the QuantERA II Programme that has received funding from the European Union's Horizon 2020 research and innovation programme under Grant Agreement No 101017733, Project No. 2021/03/Y/ST2/00195.

Appendix A: QFI for a Pure state

The generator of the interferometric transformation is $\hat{J}_y = \sum_{i=1}^M \hat{J}_y^{(i)}$. Since all $\hat{J}_y^{(i)}$'s commute, we can write the QFI as follows

$$\mathcal{I}_q = 4 \sum_{i=1}^M \Delta^2 \hat{S}_y^{(i)} + 8 \sum_{i \neq j=1}^M \left(\langle \hat{S}_y^{(i)} \hat{S}_y^{(j)} \rangle - \langle \hat{S}_y^{(i)} \rangle \langle \hat{S}_y^{(j)} \rangle \right) \quad (\text{A1})$$

The first part of the QFI simplifies to

$$\begin{aligned} 4 \sum_{i=1}^M \Delta^2 \hat{S}_y^{(i)} &= 2\Delta^2 \hat{J}_y^{(1)} + 2\Delta^2 \hat{J}_y^{(M)} + 2\langle \hat{L}^{(2)2} \rangle + 2\langle \hat{R}^{(M)2} \rangle + \\ &+ \sum_{i=2}^{M-1} \Delta^2 \hat{J}_y^{(i)} + \sum_{i=2}^{M-1} \left(\langle \hat{Y}_y^{(i)2} \rangle + \langle \hat{L}^{(i)2} \rangle + \langle \hat{R}^{(i)2} \rangle \right). \end{aligned} \quad (\text{A2})$$

The second term also simplifies, leaving the only nonzero correlations between the neighbouring operators, like $\langle \hat{L}^{(i)} \hat{R}^{(i)} \rangle$. Therefore this second part of the QFI reads

$$8 \sum_{i \neq j=1}^M \left(\langle \hat{S}_y^{(i)} \hat{S}_y^{(j)} \rangle - \langle \hat{S}_y^{(i)} \rangle \langle \hat{S}_y^{(j)} \rangle \right) = -\frac{4}{\sqrt{2}} \langle \hat{L}^{(2)} \hat{R}^{(2)} \rangle - \frac{4}{\sqrt{2}} \langle \hat{L}^{(M)} \hat{R}^{(M)} \rangle - 2 \sum_{i=3}^{M-1} \langle \hat{L}^{(i)} \hat{R}^{(i)} \rangle. \quad (\text{A3})$$

QFI for the state $|\psi\rangle$ using Eq. (A1),

$$2\Delta^2 \hat{J}_y^{(1)} = 2\Delta^2 \hat{J}_y^{(M)} = \frac{n}{2}, \quad 2\langle \hat{R}^{(i)2} \rangle = n(n+1), \quad 2\langle \hat{L}^{(i)2} \rangle = 0 \quad (\text{A4a})$$

$$\sum_{i=2}^{M-1} \Delta^2 \hat{J}_y^{(i)} = \sum_{i=2}^{M-1} \langle \hat{Y}_y^{(i)} \rangle = (M-2) \frac{n}{4} \quad (\text{A4b})$$

Hence the QFI becomes, $\mathcal{I}_q = \frac{M}{2}(n^2 + 2n) = \frac{n^2}{2M} + N$.

Using Eq. (A1), QFI for the state becomes

$$\Delta^2 \hat{J}_y^{(i)} = \frac{n}{4}, \quad \langle \hat{Y}_y^{(i)2} \rangle = \frac{n}{4}(n+1), \quad \langle \hat{R}^{(i)2} \rangle = \langle \hat{L}^{(i)2} \rangle = \frac{n}{4} \left(\frac{n}{2} + 1 \right) \quad (\text{A5a})$$

$$\langle \hat{L}^{(2)} \hat{R}^{(2)} \rangle = \langle \hat{L}^{(i)} \hat{R}^{(i)} \rangle = \langle \hat{L}^{(M)} \hat{R}^{(M)} \rangle = \frac{n^2}{8}. \quad (\text{A5b})$$

Hence the full expression for the QFI is

$$F_q = Mn\left(\frac{7+n}{8}\right) - \frac{n^2}{\sqrt{2}} + \frac{n}{2}\left(n + \frac{1}{2}\right) \quad (\text{A6})$$

QFI for the state $|\psi_\alpha\rangle$ using Eq. (A1) has a general form

$$\mathcal{I}_q = n^2 + \frac{3n}{2} + (M-2)\frac{n}{2}\left(n + \frac{3}{2}\right) - \frac{M+2}{2}\text{Re}[f] - \left(M-3 + \frac{4}{\sqrt{2}}\right)|g|^2 \quad (\text{A7})$$

where the functions f and g are defined as follows

$$g = \langle \hat{a}_r^\dagger \hat{a}_l \rangle = \frac{1}{2^n} \sum_{m=-n/2}^{n/2} e^{-i\alpha(2m+1)} \binom{n}{\frac{n}{2}-m} \binom{\frac{n}{2}-m}{2} \quad (\text{A8})$$

$$f = \langle \hat{a}_r^\dagger \hat{a}_l \hat{a}_r^\dagger \hat{a}_l \rangle = \frac{1}{2^n} \sum_{m=-\frac{n}{2}}^{\frac{n}{2}} e^{-i\alpha(2m^2+4m+4)} \times \\ \times \sqrt{\binom{n}{\frac{n}{2}+m} \binom{n}{\frac{n}{2}+m+2} \left(\frac{n}{2}+m+1\right) \binom{\frac{n}{2}-m}{2} \left(\frac{n}{2}+m+2\right) \binom{\frac{n}{2}-m-1}{2}} \quad (\text{A9})$$

Appendix B: QFI for a mixed state

The density matrix in Eq. (41) has some zero eigen values, hence the QFI must be handled with care. By labelling the non-zero eigenvalues of the density matrix with n and the zeros with n' , i.e.,

$$\hat{\rho} = \sum_{\tilde{n}} p_{\tilde{n}} |\tilde{n}\rangle \langle \tilde{n}| = \sum_n p_n |n\rangle \langle n| + \sum_{n'} 0 |n'\rangle \langle n'|. \quad (\text{B1})$$

we obtain the expression for the QFI as follows

$$\mathcal{I}_q = 2 \sum_{\tilde{n}, \tilde{m}} \frac{(p_{\tilde{n}} - p_{\tilde{m}})^2}{p_{\tilde{n}} + p_{\tilde{m}}} |\langle \tilde{n} | \hat{J}_y | \tilde{m} \rangle|^2 = 2 \sum_{n, m} \frac{(p_n - p_m)^2}{p_n + p_m} |\langle n | \hat{J}_y | m \rangle|^2 + 4 \sum_{n, m'} p_n |\langle n | \hat{J}_y | m' \rangle|^2. \quad (\text{B2})$$

The first part, we denote it by $\mathcal{I}_q^{(1)}$ is the QFI for the non-zero subspace only. Consider the second part

$$4 \sum_{n, m'} p_n |\langle n | \hat{J}_y | m' \rangle|^2 = 4 \sum_n p_n \langle n | \hat{J}_y \sum_{m'} |m'\rangle \langle m'| \hat{J}_y | n \rangle = 4 \sum_n p_n \langle n | \hat{J}_y (\hat{1} - \sum_m |m\rangle \langle m|) \hat{J}_y | n \rangle \\ = 4 \sum_n p_n \langle n | \hat{J}_y^2 | n \rangle - 4 \sum_{n, m} p_n |\langle n | \hat{J}_y | m \rangle|^2 = 4 \text{Tr}[\hat{\rho} \hat{J}_y^2] - 4 \sum_{n, m} p_n |\langle n | \hat{J}_y | m \rangle|^2. \quad (\text{B3})$$

Hence the QFI is equal to

$$\mathcal{I}_q = \mathcal{I}_q^{(1)} + 4 \text{Tr}[\hat{\rho} \hat{J}_y^2] - 4 \sum_{n, m} p_n |\langle n | \hat{J}_y | m \rangle|^2. \quad (\text{B4})$$

we now calculate the three contributions separately

$$\mathcal{I}_q^{(1)} = \sum_{ij} 2 \frac{(p_i - p_j)^2}{p_i + p_j} |\langle \psi_i | \hat{S}_y | \psi_j \rangle|^2 = \frac{1}{4} \left[\sum_{n_1, n'_1=0} \frac{(p_{n_1} - p_{n'_1})^2}{p_{n_1} + p_{n'_1}} |d[n_1, n'_1]|^2 \right. \\ \left. + \sum_{n_M, n'_M=0} \frac{(p_{n_M} - p_{n'_M})^2}{p_{n_M} + p_{n'_M}} |d[n_M, n'_M]|^2 + \sum_{n_i, n'_i=0} \frac{(p_{n_i} - p_{n'_i})^2}{p_{n_i} + p_{n'_i}} \frac{(M-2)}{2} |d[n_i, n'_i]|^2 \right]. \quad (\text{B5})$$

For clarity we use the notation $\langle n'_i, n - n'_i | \hat{S}_y | n_i, n - n_i \rangle \equiv \langle \psi'_i | \hat{S}_y | \psi_i \rangle$ where,

$$\langle \psi'_i | \hat{S}_y | \psi_i \rangle = \frac{1}{2i} (\sqrt{(n - n_i)(n_i + 1)} \delta_{n'_i = n_i + 1} - \sqrt{(n - n_i + 1)n_i} \delta_{n'_i = n_i - 1}) = \frac{1}{2i} d[n_i, n'_i]. \quad (\text{B6})$$

The second term is

$$\begin{aligned} \mathcal{I}_q^{(2)} = \sum_i 4p_{n_i} \langle \psi_i | \hat{S}_y^2 | \psi_i \rangle &= \frac{1}{2} \sum_{n_1, n_2, \dots, n_M}^n p_{n_1} p_{n_2} \dots p_{n_M} \times \\ &\times \left[\left(2n(n+2) + 2nn_1 - 2n_M^2 - 2n_1^2 + 2n_1n_2 + n_1 + n_2 - 2nn_{M-1} + 2n_Mn_{M-1} - n_{M-1} - n_M \right) \right. \\ &\left. + \frac{(M-2)}{2} \left(2n(n+2) - 2n_i^2 + 2n_in_{i+1} + 2n_{i+1} - 2n_{i-1} - 2nn_{i-1} + 2nn_{i+1} + 2n_{i-1}n_i - 2n_{i-1}n_{i+1} \right) \right] \end{aligned} \quad (\text{B7})$$

The last term reads

$$\begin{aligned} \mathcal{I}_q^{(3)} = - \sum_{ij} 4p_{n_i} |\langle \psi_i | \hat{S}_y | \psi_j \rangle|^2 &= -\frac{1}{2} \left[\sum_{n_1, n'_1=0} p_{n_1} |d[n_1, n'_1]|^2 \right. \\ &\left. + \sum_{n_M, n'_M=0} p_{n_M} |d[n_M, n'_M]|^2 + \sum_{n_i, n'_i=0} p_{n_i} \frac{(M-2)}{2} |d[n_i, n'_i]|^2 \right] \end{aligned} \quad (\text{B8})$$

Furthermore, we observe that the first term $\mathcal{I}_q^{(1)}$ vanishes. The terms $\mathcal{I}_q^{(2)}$ and $\mathcal{I}_q^{(3)}$ results for large σ in

$$\begin{aligned} \mathcal{I}_q = \left(\frac{11M-2}{12} \right) \left(\frac{n^2}{2} + n \right) &- \frac{1}{2(n+1)} \left(\sum_{n_1, n'_1=0} |d[n_1, n'_1]|^2 \right. \\ &\left. + \sum_{n_M, n'_M=0} |d[n_M, n'_M]|^2 + \frac{M-2}{2} \sum_{n_i, n'_i=0} |d[n_i, n'_i]|^2 \right). \end{aligned} \quad (\text{B9})$$

The summations can be performed analytically giving

$$\sum_{n_1, n'_1=0} |d[n_1, n'_1]|^2 = \sum_{n_M, n'_M=0} |d[n_M, n'_M]|^2 = \sum_{n_i, n'_i=0} |d[n_i, n'_i]|^2 = \frac{1}{3}(n^3 + 3n^2 + 2n), \quad (\text{B10})$$

resulting in a simplified expression for the QFI,

$$\mathcal{I}_q(\sigma \rightarrow \infty) = \frac{n^2 + 2n}{8}(3M-2), \quad (\text{B11})$$

as reported in the main text.

-
- [1] S. L. Braunstein and C. M. Caves, Statistical distance and the geometry of quantum states, *Physical Review Letters* **72**, 3439 (1994).
 - [2] A. Holevo, *Probabilistic and Statistical Aspects of Quantum Theory* (Publications of Scuola Normale Superiore, 2011).
 - [3] V. Giovannetti, S. Lloyd, and L. Maccone, Quantum-enhanced measurements: beating the standard quantum limit, *Science* **306**, 1330 (2004).
 - [4] B. P. Abbott, R. Abbott, T. D. Abbott, M. R. Abernathy, F. Acernese, K. Ackley, C. Adams, T. Adams, P. Addesso, R. X. Adhikari, *et al.*, Observation of gravitational waves from a binary black hole merger, *Physical review letters* **116**, 061102 (2016).
 - [5] G. Ferrari, N. Poli, F. Sorrentino, and G. M. Tino, Long-lived bloch oscillations with bosonic sr atoms and application to gravity measurement at the micrometer scale, *Phys. Rev. Lett.* **97**, 060402 (2006).
 - [6] N. Poli, F.-Y. Wang, M. G. Tarallo, A. Alberti, M. Prevedelli, and G. M. Tino, Precision measurement of gravity with cold atoms in an optical lattice and comparison with a classical gravimeter, *Phys. Rev. Lett.* **106**, 038501 (2011).
 - [7] G. W. Biedermann, X. Wu, L. Deslauriers, S. Roy, C. Maheswaraswamy, and M. A. Kasevich, Testing gravity with cold-atom interferometers, *Phys. Rev. A* **91**, 033629 (2015).
 - [8] B. Dubetsky and M. A. Kasevich, Atom interferometer as a selective sensor of rotation or gravity, *Phys. Rev. A* **74**, 023615 (2006).
 - [9] J. M. McGuirk, G. T. Foster, J. B. Fixler, M. J. Snadden, and M. A. Kasevich, Sensitive absolute-gravity gradiometry using atom interferometry, *Phys. Rev. A* **65**, 033608 (2002).
 - [10] M. Kasevich and S. Chu, Measurement of the gravitational acceleration of an atom with a light-pulse atom

- interferometer, *Applied Physics B* **54**, 321 (1992).
- [11] J. B. Fixler, G. T. Foster, J. M. McGuirk, and M. A. Kasevich, Atom interferometer measurement of the newtonian constant of gravity, *Science* **315**, 74 (2007), <https://www.science.org/doi/pdf/10.1126/science.1135459>.
 - [12] M. Fattori, C. D’Errico, G. Roati, M. Zaccanti, M. Jonas-Lasinio, M. Modugno, M. Inguscio, and G. Modugno, Atom interferometry with a weakly interacting bose-einstein condensate, *Phys. Rev. Lett.* **100**, 080405 (2008).
 - [13] K. Jachymski, T. Wasak, Z. Idziaszek, P. S. Julienne, A. Negretti, and T. Calarco, Single-atom transistor as a precise magnetic field sensor, *Phys. Rev. Lett.* **120**, 013401 (2018).
 - [14] J. A. Dunningham and K. Burnett, Sub-shot-noise-limited measurements with bose-einstein condensates, *Phys. Rev. A* **70**, 033601 (2004).
 - [15] L. Pezzé and A. Smerzi, Entanglement, nonlinear dynamics, and the Heisenberg limit, *Phys. Rev. Lett.* **102**, 100401 (2009).
 - [16] B. Yadin, M. Fadel, and M. Gessner, Metrological complementarity reveals the einstein-podolsky-rosen paradox, *Nature communications* **12**, 2410 (2021).
 - [17] A. Niezgoda and J. Chwedeńczuk, Many-body nonlocality as a resource for quantum-enhanced metrology, *Phys. Rev. Lett.* **126**, 210506 (2021).
 - [18] F. Fröwis, M. Fadel, P. Treutlein, N. Gisin, and N. Brunner, Does large quantum fisher information imply bell correlations?, *Phys. Rev. A* **99**, 040101 (2019).
 - [19] C. C. Gerry and R. A. Campos, Generation of maximally entangled states of a bose-einstein condensate and heisenberg-limited phase resolution, *Phys. Rev. A* **68**, 025602 (2003).
 - [20] R. Demkowicz-Dobrzański, J. Kołodyński, and M. Guta, The elusive heisenberg limit in quantum-enhanced metrology, *Nat. Commun.* **3**, 1063 (2012).
 - [21] T. Schumm, S. Hofferberth, L. M. Andersson, S. Wildermuth, S. Groth, I. Bar-Joseph, J. Schmiedmayer, and P. Krüger, Matter-wave interferometry in a double well on an atom chip, *Nat. Phys.* **1**, 57 (2005).
 - [22] G.-B. Jo, Y. Shin, S. Will, T. Pasquini, M. Saba, W. Ketterle, D. Pritchard, M. Vengalattore, and M. Prentiss, Long phase coherence time and number squeezing of two bose-einstein condensates on an atom chip, *Phys. Rev. Lett.* **98**, 030407 (2007).
 - [23] P. Böhi, M. F. Riedel, J. Hoffrogge, J. Reichel, T. W. Hänsch, and P. Treutlein, Coherent manipulation of bose-einstein condensates with state-dependent microwave potentials on an atom chip, *Nat. Phys.* **5**, 592 (2009).
 - [24] J. Esteve, C. Gross, A. Weller, S. Giovanazzi, and M. Oberthaler, Squeezing and entanglement in a Bose-Einstein condensate, *Nature* **455**, 1216 (2008).
 - [25] Y. Huang and M. Moore, Optimized double-well quantum interferometry with gaussian squeezed states, *Phys. Rev. Lett.* **100**, 250406 (2008).
 - [26] I. D. Leroux, M. H. Schleier-Smith, and V. Vuletić, Orientation-dependent entanglement lifetime in a squeezed atomic clock, *Phys. Rev. Lett.* **104**, 250801 (2010).
 - [27] Z. Chen, J. G. Bohnet, S. R. Sankar, J. Dai, and J. K. Thompson, Conditional spin squeezing of a large ensemble via the vacuum rabi splitting, *Phys. Rev. Lett.* **106**, 133601 (2011).
 - [28] T. Berrada, S. van Frank, R. Bücke, T. Schumm, J.-F. Schaff, and J. Schmiedmayer, Integrated mach-zehnder interferometer for bose-einstein condensates, *Nat. Commun.* **4** (2013).
 - [29] R. Bücke, J. Grond, S. Manz, T. Berrada, T. Betz, C. Koller, U. Hohenester, T. Schumm, A. Perrin, and J. Schmiedmayer, Twin-atom beams, *Nat. Phys.* **7**, 608 (2011).
 - [30] K. V. Kheruntsyan, J.-C. Jaskula, P. Deuar, M. Bonneau, G. B. Partridge, J. Ruauudel, R. Lopes, D. Boiron, and C. I. Westbrook, Violation of the cauchy-schwarz inequality with matter waves, *Phys. Rev. Lett.* **108**, 260401 (2012).
 - [31] A. Perrin, H. Chang, V. Krachmalnicoff, M. Schellekens, D. Boiron, A. Aspect, and C. I. Westbrook, Observation of atom pairs in spontaneous four-wave mixing of two colliding bose-einstein condensates, *Phys. Rev. Lett.* **99**, 150405 (2007).
 - [32] M. Bonneau, J. Ruauudel, R. Lopes, J.-C. Jaskula, A. Aspect, D. Boiron, and C. I. Westbrook, Tunable source of correlated atom beams, *Phys. Rev. A* **87**, 061603 (2013).
 - [33] J. M. Vogels, K. Xu, and W. Ketterle, Generation of macroscopic pair-correlated atomic beams by four-wave mixing in bose-einstein condensates, *Phys. Rev. Lett.* **89**, 020401 (2002).
 - [34] W. RuGway, S. S. Hodgman, R. G. Dall, M. T. Johnsson, and A. G. Truscott, Correlations in amplified four-wave mixing of matter waves, *Phys. Rev. Lett.* **107**, 075301 (2011).
 - [35] D. K. Shin, B. M. Henson, S. S. Hodgman, T. Wasak, J. Chwedeńczuk, and A. G. Truscott, Bell correlations between spatially separated pairs of atom, *Nat. Comm.* **10**, 4447 (2019).
 - [36] B. Lücke, J. Peise, G. Vitagliano, J. Arlt, L. Santos, G. Tóth, and C. Klempt, Detecting multiparticle entanglement of dicke states, *Phys. Rev. Lett.* **112**, 155304 (2014).
 - [37] B. Lücke, M. Scherer, J. Kruse, L. Pezzé, F. Deuretzbacher, P. Hyllus, O. Topic, J. Peise, W. Ertmer, J. Arlt, L. Santos, A. Smerzi, and C. Klempt, Twin matter waves for interferometry beyond the classical limit, *Science* **334**, 773 (2011), <https://www.science.org/doi/pdf/10.1126/science.1208798>.
 - [38] D. C. Burnham and D. L. Weinberg, Observation of simultaneity in parametric production of optical photon pairs, *Phys. Rev. Lett.* **25**, 84 (1970).
 - [39] P. G. Kwiat, K. Mattle, H. Weinfurter, A. Zeilinger, A. V. Sergienko, and Y. Shih, New high-intensity source of polarization-entangled photon pairs, *Phys. Rev. Lett.* **75**, 4337 (1995).
 - [40] A. Peters, K. Y. Chung, and S. Chu, High-precision gravity measurements using atom interferometry, *Metrologia* **38**, 25 (2001).
 - [41] G. M. Tino, Testing gravity with cold atom interferometry: results and prospects, *Quantum Science and Technology* **6**, 024014 (2021).
 - [42] A. Peters, K. Y. Chung, and S. Chu, Measurement of gravitational acceleration by dropping atoms, *Nature* **400**, 849 (1999).
 - [43] A. Peters, K. Y. Chung, and S. Chu, High-precision gravity measurements using atom interferometry, *Metrologia* **38**, 25 (2001).
 - [44] D. S. Weiss, B. C. Young, and S. Chu, Precision measurement of \hbar/m cs based on photon recoil using laser-cooled

- atoms and atomic interferometry, *Applied physics B* **59**, 217 (1994).
- [45] P. A. Altin, M. T. Johnsson, V. Negnevitsky, G. R. Dennis, R. P. Anderson, J. E. Debs, S. S. Szigeti, K. S. Hardman, S. Bennetts, G. D. McDonald, L. D. Turner, J. D. Close, and N. P. Robins, Precision atomic gravimeter based on bragg diffraction, *New Journal of Physics* **15**, 023009 (2013).
 - [46] L. Masi, T. Petrucciani, G. Ferioli, G. Semeghini, G. Modugno, M. Inguscio, and M. Fattori, Spatial bloch oscillations of a quantum gas in a “beat-note” superlattice, *Physical Review Letters* **127**, 020601 (2021).
 - [47] T. Petrucciani, A. Santoni, C. Mazzinghi, D. Trypogeorgos, F. S. Cataliotti, M. Inguscio, G. Modugno, A. Smerzi, L. Pezzé, and M. Fattori, Mach-zehnder atom interferometry with non-interacting trapped bose einstein condensates, *arXiv preprint arXiv:2504.17391* (2025).
 - [48] C. K. Hong, Z. Y. Ou, and L. Mandel, Measurement of subpicosecond time intervals between two photons by interference, *Phys. Rev. Lett.* **59**, 2044 (1987).
 - [49] M. Płodzień, M. Lewenstein, E. Witkowska, and J. Chwedeńczuk, One-axis twisting as a method of generating many-body bell correlations, *Physical Review Letters* **129**, 250402 (2022).
 - [50] C. Gerry and P. Knight, *Introductory Quantum Optics* (Cambridge University Press, 2004).
 - [51] R. Lopes, A. Imanaliev, A. Aspect, M. Cheneau, D. Boiron, and C. I. Westbrook, Atomic hong-ou-mandel experiment, *Nature* **520**, 66 (2015).
 - [52] N. Killoran, M. Cramer, and M. B. Plenio, Extracting entanglement from identical particles, *Phys. Rev. Lett.* **112**, 150501 (2014).
 - [53] J. Beugnon, M. P. A. Jones, J. Dingjan, B. Darquié, G. Messin, A. Browaeys, and P. Grangier, Quantum interference between two single photons emitted by independently trapped atoms, *Nature* **440**, 779 (2006).
 - [54] B. Yurke and D. Stoler, Bell’s-inequality experiments using independent-particle sources, *Phys. Rev. A* **46**, 2229 (1992).
 - [55] T. Wasak, P. Szańkowski, and J. Chwedeńczuk, Interferometry with independently prepared Bose-Einstein condensates, *Phys. Rev. A* **91**, 043619 (2015).